Title
Imaging of point scatterers from step-frequency ISAR data

Journal
IEEE Transactions on Aerospace and Electronic Systems, 29(1)

ISSN
0018-9251

Authors
Hua, Y
Baqai, FA
Zhu, Y
et al.

Publication Date
1993

DOI
10.1109/7.249125

Peer reviewed

Imaging of Point Scatterers from Step-Frequency ISAR Data

Y. HUA, Senior Member, IEEE

F. BAQAI

Y. ZHU
University of Melbourne

D. HEILBRONN
Surveillance Research Laboratory
Australia

We present a high resolution method for imaging of point scatterers from step-frequency inverse synthetic aperture radar (ISAR) data. An analysis of the noise sensitivity of the method is provided to show the high performance of the method. Simulation results are given to show the robustness of the method against model errors.

Manuscript received September 9, 1991; revised December 17, 1991.

IEEE Log No. T-AES/29/1/03782.

This work was supported by the Australian Research Council and the Defence Science and Technology Organization of Australia.

Authors' addresses: Y. Hua, F. Baqai, Y. Zhu, Dept. of Electrical and Electronic Engineering, University of Melbourne, Parkville, Victoria 3052, Australia; D. Heilbronn, Surveillance Research Laboratory, DSTO Salisbury, P.O. Box 1650, South Australia 5108, Australia.

0018-9251/93/$3.00

I. INTRODUCTION

This work describes a signal processing technique for imaging of point scatterers from step-frequency inverse synthetic aperture radar (ISAR [1, 2]) data. The point scatterers are assumed to form a target that is moving with respect to a stationary radar. The radar transmits towards the target a sequence of pulses at different frequencies and receives the corresponding returns. From the radar returns, our technique yields the accurate estimates of the locations of the point scatterers.

The traditional method for target imaging from ISAR data is the fast Fourier transform (FFT) method [1]. The FFT method is known to yield poor resolution if the "aperture" spanned by the collected data is not large enough. In the ISAR applications, large aperture data set (or large time-interval data set) often contains large distortions caused by the moving target. To reduce the (often unknown) motion distortions, it is desired to obtain the target image from a small aperture data set. Given a small aperture data set, the FFT method cannot yield a high resolution image. We present here a new method called the matrix pencil (MP) method which can cope with a small aperture data set and yield a high resolution image. The computation of this method is also efficient compared with other available high resolution methods.

This paper is organized as follows. In Section II, a model of the ISAR data is established. In Section III, the MP method is developed. In Section IV, a noise sensitivity analysis of the MP method is shown. In Section V, simulation results are provided.

II. THE ISAR DATA MODEL

The following assumptions are made throughout this paper.

Assumption 1: The (rigid) target consists of point scatterers, and the reflection coefficient of each scatterer is a (complex) constant.

Assumption 2: The target is far away from the radar.

With the above two assumptions, each narrowband pulse received by the radar (after being normalized by the transmitted signal) can be represented by complex envelope:

$$s(\theta,f) = \sum_{i=1}^{I} a_i \exp\left(-j\frac{4\pi}{c}f(d + x_i\cos\theta - y_i\sin\theta)\right) \tag{1}$$

where θ denotes the angle position of the target (see Fig. 1) which is assumed to be constant during the (very short) interval of each pulse, f the carrier frequency of each narrowband pulse, a_i the reflection coefficient of the ith scatterer, I the total number of point scatterers, c the wave velocity, d the distance

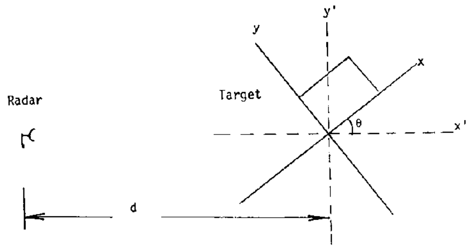

Fig. 1. Coordinates of moving target with respect to radar.

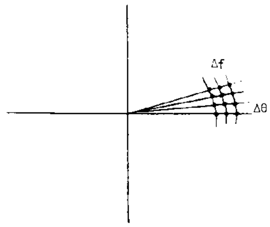

Fig. 2. Grid on which step-frequency ISAR data is located.

between the radar and the target, and (x_i, y_i) the coordinates of the ith point scatterer.

The imaging objective here is to find a_i and (x_i, y_i) from $s(\theta, f)$ available on a given set of sample points of θ and f. Finding a_i is relatively an easy task once (x_i, y_i) are available because $f(\theta, f)$ is a linear function of a_i. But finding (x_i, y_i) from $s(\theta, f)$ is much more difficult. To make the problem simpler, we further assume the following.

Assumption 3: The distance between the target and the radar is known so that the phase due to the distance can be suppressed from $s(\theta, f)$.

Assumption 4: For each angular position of the target, a sequence of narrowband pulses at the carrier frequencies $f_m = f_L + m\Delta f$ for $m = 0, 1, \ldots, M-1$ are transmitted by the radar, and the corresponding returns are received.

Assumption 5: The target takes the angular positions $\theta_n = n\Delta\theta$ for $n = 0, 1, \ldots, N-1$.

The above assumptions imply that the measured ISAR data is a sampled Fourier transform of the target reflection function, i.e., sampled on the polar coordinates as shown in Fig. 2. To make the ISAR data structure even simpler, further restrictions are imposed on the radar as follows.

Assumption 6: The frequency interval $M\Delta f$ is much smaller than the middle frequency $f_0 = f_i + (M-1)\Delta f/2$.

Assumption 7: The angular interval $N\Delta\theta$ is much smaller than one.

The last two assumptions imply that the sampled region (wedge) shown in Fig. 2 becomes approximately rectangular. It should be noted that assumptions 4 and 5 cannot be met if the target is continuously rotating (rather than in the stepped format). But for simple analysis these two assumptions are used until Section V where a continuously rotating target is considered.

By combining assumptions 3–7, a simple analysis can transform (1) into

$$s(m,n) = \sum_{i=1}^{I} b_i \exp(j2\pi f_{xi} m + j2\pi f_{yi} n)$$

$$= \sum_{i=1}^{I} b_i p_i^m q_i^n \tag{2}$$

where

$$b_i = a_i \exp\left(-j\frac{4\pi}{c} x_i f_L\right) \tag{3}$$

$$f_{xi} = -\frac{2}{c}\Delta f\, x_i \tag{4}$$

$$f_{yi} = \frac{2}{c} f_0 \Delta\theta\, y_i \tag{5}$$

$$p_i = \exp(j2\pi f_{xi}) \tag{6}$$

$$q_i = \exp(j2\pi f_{yi}). \tag{7}$$

The model shown in (2) is simply a sum of 2-D (two-dimensional) complex sinusoids with the 2-D frequencies at (f_{xi}, f_{yi}). Note that Δf and $\Delta\theta$ must be such that $-0.5 < f_{xi} < 0.5$ and $-0.5 < f_{yi} < 0.5$ to avoid phase ambiguity. Since (x_i, y_i) can be uniquely obtained from (f_{xi}, f_{yi}) by using (4) and (5), we discuss the estimation of (f_{xi}, f_{yi}) only.

It should be noted that the assumptions made above are similar to those in [1], and hence the model shown in (2) is similar to that used in [1]. But in [1], the target is assumed to be spatially bandlimited (i.e., the target is smooth). Here, we are treating a target that consists of point scatterers which are not bandlimited in spatial frequency. Although the 2-D FFT technique proposed in [1] can be applied here, it has poor resolution because the data aperture can be very small under assumptions 6 and 7.

In the next section, a high resolution method for estimating (f_{xi}, f_{yi}) is developed based on the model shown in (2).

III. THE MATRIX PENCIL METHOD

The *first* step of the MP method is to form the enhanced matrix:

$$\mathbf{S}_e = \begin{bmatrix} \mathbf{S}_0 & \mathbf{S}_1 & \cdots & \mathbf{S}_{M-K} \\ \mathbf{S}_1 & \mathbf{S}_2 & \cdots & \mathbf{S}_{M-K+1} \\ \cdots & \cdots & \cdots & \cdots \\ \mathbf{S}_{K-1} & \mathbf{S}_K & \cdots & \mathbf{S}_{M-1} \end{bmatrix} \tag{8}$$

where $\{\mathbf{S}_m;\ m=0,1,\cdots,M-1\}$ are defined by

$$\mathbf{S}_m=\begin{bmatrix} s(m;0) & s(m;1) & \cdots & s(m;N-L) \\ s(m;1) & s(m;2) & \cdots & s(m;N-L+1) \\ \cdots & \cdots & \cdots & \cdots \\ s(m;L-1) & s(m;L) & \cdots & s(m;N-1) \end{bmatrix}. \tag{9}$$

Note that we have introduced the two integers K and L in the above two equations. The integer K may be called the moving window length in the m (or f_x) direction, and L the moving window length in the n (or f_y) direction. The conditions which need to be satisfied by K and L will be given later.

The *second* step of the MP method is to compute the singular value decomposition (SVD) of $\mathbf{S}_e$:

$$\mathbf{S}_e=\mathbf{U}\Sigma\mathbf{V}^{\mathrm{H}} \tag{10}$$

where $\mathbf{U}=[\mathbf{u}_1,\mathbf{u}_2,\ldots,\mathbf{u}_{\min}]$ consists of the left singular vectors, $\mathbf{V}=[\mathbf{v}_1,\mathbf{v}_2,\ldots,\mathbf{v}_{\min}]$ consists of the right singular vectors, and $\Sigma=\mathrm{diag}(\sigma_1,\sigma_2,\ldots\sigma_{\min})$ consists of the (descending) singular values; min is the smaller one of the column and row dimensions of $\mathbf{S}_e$, i.e., $\min(KL,(M-K+1)(N-L+1))$. Note that the right singular vectors are not required by the MP method. Therefore, one can simply use the eigendecomposition of the Hermitian matrix $\mathbf{S}_e\mathbf{S}_e^{\mathrm{H}}$ which can be decomposed into $\mathbf{U}\Sigma^2\mathbf{U}$.

To relate the SVD to the data structure shown in (2), we use (2) in (9) to yield

$$\mathbf{S}_m=\mathbf{Q}_c\mathbf{B}\mathbf{P}_d^m\mathbf{Q}_r \tag{11}$$

where

$$\mathbf{Q}_c=\begin{bmatrix} 1 & 1 & \cdots & 1 \\ q_1 & q_2 & \cdots & q_I \\ \cdots & \cdots & \cdots & \cdots \\ q_1^{L-1} & q_2^{L-1} & \cdots & q_I^{L-1} \end{bmatrix} \tag{12}$$

$$\mathbf{B}=\mathrm{diag}(b_1,b_2,\ldots,b_I) \tag{13}$$

$$\mathbf{P}_d=\mathrm{diag}(p_1,p_2,\ldots,p_I) \tag{14}$$

$$\mathbf{Q}_r=\begin{bmatrix} 1 & q_1 & \cdots & q_1^{N-L} \\ 1 & q_2 & \cdots & q_2^{N-L} \\ \cdots & \cdots & \cdots & \cdots \\ 1 & q_I & \cdots & q_I^{N-L} \end{bmatrix}. \tag{15}$$

Then using (11) in (8) yields

$$\mathbf{S}_e=\mathbf{E}_c\mathbf{B}\mathbf{E}_r \tag{16}$$

where

$$\mathbf{E}_c=\begin{bmatrix} \mathbf{Q}_c \\ \mathbf{Q}_c\mathbf{P}_d \\ \cdots \\ \mathbf{Q}_c\mathbf{P}_d^{K-1} \end{bmatrix} \tag{17}$$

$$\mathbf{E}_r=[\mathbf{Q}_r,\mathbf{P}_d\mathbf{Q}_r,\cdots,\mathbf{P}_d^{M-K}\mathbf{Q}_r]. \tag{18}$$

By using the above decompositions, we can show [3] that if*

$$\begin{cases} I+1\le K\le M-I+1 \\ I+1\le L\le N-I+1 \end{cases} \tag{19}$$

then $\mathrm{rank}(\mathbf{E}_c)=I$, $\mathrm{rank}(\mathbf{E}_r)=I$ and hence $\mathrm{rank}(\mathbf{S}_e)=I$ which implies

$$\sigma_i=\begin{cases} >0 & \text{for } i\le I \\ 0 & \text{for } i>I \end{cases}. \tag{20}$$

Because of the above property, the *third* step of the MP method is to choose such I that σ_i for $i>I$ are negligible compared with σ_i for $i\le I$.

Because of (20), (16), and (10), we know that

$$\mathrm{range}(\mathbf{S}_e)=\mathrm{range}(\mathbf{E}_c)=\mathrm{range}(\mathbf{U}_s) \tag{21}$$

where

$$\mathbf{U}_s=[\mathbf{u}_1,\mathbf{u}_2,\ldots,\mathbf{u}_I]. \tag{22}$$

Then it follows that $\mathrm{range}(\mathbf{E}_c)$ is orthogonal to $\mathrm{range}(\mathbf{U}_n)$, i.e.,

$$\mathrm{range}(\mathbf{E}_c)\perp\mathrm{range}(\mathbf{U}_n) \tag{23}$$

where

$$\mathbf{U}_n=[\mathbf{u}_{I+1},\mathbf{u}_{I+2},\ldots,\mathbf{u}_{\min}]. \tag{24}$$

From (17) we know that

$$\mathbf{E}_c=[\mathbf{e}(f_{x1},f_{y1}),\mathbf{e}(f_{x2},f_{y2}),\ldots,\mathbf{e}(f_{xI},f_{yI})] \tag{25}$$

where

$$\mathbf{e}(f_{xi},f_{yi})=\begin{bmatrix} 1 \\ q_i \\ \cdots \\ q_i^{L-1} \\ p_i \\ p_iq_i \\ \cdots \\ p_iq_i^{L-1} \\ \cdots \\ \cdots \\ p_i^{K-1} \\ p_i^{K-1}q_i \\ \cdots \\ p_i^{K-1}q_i^{L-1} \end{bmatrix} = \begin{bmatrix} 1 \\ p_i \\ \cdots \\ p_i^{K-1} \end{bmatrix} \otimes \begin{bmatrix} 1 \\ q_i \\ \cdots \\ q_i^{L-1} \end{bmatrix} \tag{26}$$

in which $\otimes$ denotes the Kronecker product. Combining

*This condition combines that for E_1 and E_2 as defined in (28) and (30) to be of the rank 2.

(23) and (25) yields that for $i = I+1, I+2, \ldots, \min$,

$$\mathbf{u}_i^{\mathrm{H}}\mathbf{e}(f_{xi}, f_{yi}) = 0. \tag{27}$$

This property implies that one can use the following 2-D spectrum to find the 2-D frequencies (f_{xi}, f_{yi}):

$$P(f_x, f_y) = \frac{1}{\sum_{i=I+1}^{\min} |\mathbf{u}_i^{\mathrm{H}}\mathbf{e}(f_x, f_y)|^2}. \tag{28}$$

This spectrum has higher resolution than the 2-D FFT as used in [1] because the peak positions of $P(f_x, f_y)$ are guaranteed by (27) (in the noiseless case) to be the true scatterer positions. But the computation required to obtain the 2-D frequencies (f_{xi}, f_{yi}) from the 2-D spectrum is often an excessive burden [4, 5].

To develop a computationally efficient way, we define the following:

$$\mathbf{E}_1 = \mathbf{E}_c \text{ with the last } L \text{ rows deleted} \tag{29}$$

$$\mathbf{E}_2 = \mathbf{E}_c \text{ with the first } L \text{ rows deleted} \tag{30}$$

$$\mathbf{U}_1 = \mathbf{U}_s \text{ with the last } L \text{ rows deleted} \tag{31}$$

$$\mathbf{U}_2 = \mathbf{U}_s \text{ with the first } L \text{ rows deleted.} \tag{32}$$

Then it follows from (21) that

$$\mathbf{U}_1 = \mathbf{E}_1\mathbf{T} \tag{33}$$

$$\mathbf{U}_2 = \mathbf{E}_2\mathbf{T} \tag{34}$$

where $\mathbf{T}$ is a nonsingular square matrix. Applying (17), we have

$$\begin{aligned} \mathbf{U}_2 - p\mathbf{U}_1 &= (\mathbf{E}_2 - p\mathbf{E}_1)\mathbf{T} \\ &= \mathbf{E}_1(\mathbf{P}_d - p\mathbf{I})\mathbf{T} \end{aligned} \tag{35}$$

where $\mathbf{I}$ is the identity matrix with proper dimension. This equation implies [7] that p_i for $i = 1, 2, \ldots, I$ are the generalized eigenvalues of the MP $\mathbf{U}_2 - p\mathbf{U}_1$, i.e., $\mathbf{U}_2 - p\mathbf{U}_1$ decreases its rank by one if and only if $p = p_i$, provided that (19) is satisfied.

To study q_i for $i = 1, 2, \ldots, I$, we first define the shuffling matrix:

$$\mathbf{P}_s = \begin{bmatrix} \mathbf{p}^T(1) \\ \mathbf{p}^T(1+L) \\ \cdots \\ \mathbf{p}^T(1+(K-1)L) \\ \mathbf{p}^T(2) \\ \mathbf{p}^T(2+L) \\ \cdots \\ \mathbf{p}^T(2+(K-1)L) \\ \cdots \\ \cdots \\ \mathbf{p}^T(L) \\ \mathbf{p}^T(L+L) \\ \cdots \\ \mathbf{p}^T(L+(K-1)L) \end{bmatrix} \tag{36}$$

where $\mathbf{p}^T(i)$ is the $1 \times KL$ vector with one at the ith position and zero everywhere else. Then the shuffled matrix $\mathbf{E}_c' = \mathbf{P}_s\mathbf{E}_c$ of $\mathbf{E}_c$ can be written as (see (17))

$$\mathbf{E}_c' = \begin{bmatrix} \mathbf{P}_c \\ \mathbf{P}_c\mathbf{Q}_d \\ \cdots \\ \mathbf{P}_c\mathbf{Q}_d^{L-1} \end{bmatrix} \tag{37}$$

where

$$\mathbf{P}_c = \begin{bmatrix} 1 & 1 & \cdots & 1 \\ p_1 & p_2 & \cdots & p_I \\ \cdots & \cdots & \cdots & \cdots \\ p_1^{K-1} & p_2^{K-1} & \cdots & p_I^{K-1} \end{bmatrix} \tag{38}$$

$$\mathbf{Q}_d = \mathrm{diag}(q_1, q_2, \ldots, q_I). \tag{39}$$

Similar to (29)–(32), we define

$$\mathbf{E}_1' = \mathbf{E}_c' \text{ with the last } K \text{ rows deleted} \tag{40}$$

$$\mathbf{E}_2' = \mathbf{E}_c' \text{ with the first } K \text{ rows deleted} \tag{41}$$

$$\mathbf{U}_1' = \mathbf{P}_s\mathbf{U}_s \text{ with the last } K \text{ rows deleted} \tag{42}$$

$$\mathbf{U}_2' = \mathbf{P}_s\mathbf{U}_s \text{ with the first } K \text{ rows deleted.} \tag{43}$$

Then we have, similar to (35),

$$\mathbf{U}_2' - q\mathbf{U}_1' = \mathbf{E}_1'(\mathbf{Q}_d - q\mathbf{I})\mathbf{T}. \tag{44}$$

This equation implies [7] that q_i for $i = 1, 2, \ldots, I$ are the generalized eigenvalues of the MP $\mathbf{U}_2' - q\mathbf{U}_1'$.

Based on the above analysis, the *fourth* step of the MP method is to form $\mathbf{U}_1$, $\mathbf{U}_2$, $\mathbf{U}_1'$, and $\mathbf{U}_2'$ according to (31), (32), (42), and (43), respectively, and then obtain the estimates of p_i and q_i by computing the generalized eigenvalues of $\mathbf{U}_2 - p\mathbf{U}_1$ and $\mathbf{U}_2' - q\mathbf{U}_1'$, respectively. The generalized eigenvalue problem can be solved in a number of ways [6]. But the simplest way is to compute the eigenvalues of $(\mathbf{U}_1^{\mathrm{H}}\mathbf{U}_1)^{-1}\mathbf{U}_1^{\mathrm{H}}\mathbf{U}_2$ and $(\mathbf{U}_1'^{\mathrm{H}}\mathbf{U}_1')^{-1}\mathbf{U}_1'^{\mathrm{H}}\mathbf{U}_2'$ [8] for p_i and q_i, respectively.

The *fifth* step of the MP method is to convert p_i and q_i to f_{xi} and f_{yi} according to (6) and (7), i.e.,

$$f_{xi} = \frac{1}{2\pi}\mathrm{Im}[\log(p_i)] \tag{45}$$

$$f_{yi} = \frac{1}{2\pi}\mathrm{Im}[\log(q_i)]. \tag{46}$$

The *sixth* (i.e., final) step of the MP method is to have the estimated f_{xi} and f_{yi} correctly paired. An efficient pairing technique is to use (28), e.g., for each i, choose j such that $P(f_{xi}, f_{yj})$ is maximum.

It is important to note that the MP method becomes more robust to noise when the enhanced matrix $\mathbf{S}_e$ is replaced by the expanded matrix:

$$\mathbf{S}_{efb} = [\mathbf{S}_e, \mathbf{P}_p\mathbf{S}_e^*] \tag{47}$$

where * denotes the conjugation, and $\mathbf{P}_p$ is the permutation matrix with ones on the cross diagonal axis. In the following two sections, only the expanded matrix is used. (The analysis of $\mathbf{S}_{efb}$ leading to the above shown steps of the MP method would be similar.)

Also note that the conditions (19) on K and L are sufficient for the MP method to yield the exact esitmates of (f_{xi}, f_{yi}) in the noiseless case. Both K and L affect the noise sensitivity greatly, which is shown next.

IV. NOISE SENSITIVITY

In this section, we consider the noise sensitivity of the MP method. In particular, we discuss the effect of K and L on the noise sensitivity and compare the noise sensitivity with the Cramer-Rao lower bound (CRB) [9].

A. Derivation of First-Order Perturbations

It is clear that the first-order perturbations in the estimated f_{xi} and f_{yi} can be expressed by

$$\Delta f_{xi} = \epsilon_{xi1}^T \mathrm{Re}[\mathbf{w}] + \epsilon_{xi2}^T \mathrm{Im}[\mathbf{w}] \tag{48}$$

$$\Delta f_{yi} = \epsilon_{yi1}^T \mathrm{Re}[\mathbf{w}] + \epsilon_{yi2}^T \mathrm{Im}[\mathbf{w}] \tag{49}$$

where $\mathbf{w}$ is the noise vector defined by

$$\mathbf{w} = \begin{bmatrix} w(0;0) \\ w(0;1) \\ \cdots \\ w(0;N-1) \\ w(1;0) \\ w(1;1) \\ \cdots \\ w(1;N-1) \\ \cdots \\ \cdots \\ w(M-1;0) \\ w(M-1;1) \\ \cdots \\ w(M-1;N-1) \end{bmatrix} \tag{50}$$

and ϵ_{xi1}, ϵ_{xi2}, ϵ_{yi1}, and ϵ_{yi2} are the noise sensitivity vectors. In the following, we derive the detailed expressions for these vectors, but since Δf_{xi} and Δf_{yi} can be treated symmetrically, we concentrate on Δf_{xi}.

From (45), it is clear that

$$\Delta f_{xi} = \frac{1}{2\pi} \mathrm{Im}\left[\frac{\Delta p_i}{p_i}\right]. \tag{51}$$

Based on the fourth step of the MP method, we know that Δp_i is the perturbation in the ith generalized eigenvalue of the MP $\mathbf{U}_2 - p\mathbf{U}_1$. By applying the theorem that "the SVD truncation does not affect the first-order perturbations" as shown in [6], it can be shown that Δp_i is equal to the perturbation in the ith generalized eigenvalue of the MP $\mathbf{S}_2 - p\mathbf{S}_1$ where

$$\mathbf{S}_1 = \mathbf{S}_{efb} \text{ with the last } L \text{ rows deleted} \tag{52}$$

$$\mathbf{S}_2 = \mathbf{S}_{efb} \text{ with the first } L \text{ rows deleted.} \tag{53}$$

Then it follows [7] that

$$\Delta p_i = \frac{\mathbf{p}_i^{\mathrm{H}}(\Delta\mathbf{S}_2 - p_i\Delta\mathbf{S}_1)\mathbf{q}_i}{\mathbf{p}_i^{\mathrm{H}}\mathbf{S}_1\mathbf{q}_i} \tag{54}$$

where $\mathbf{p}_i$ and $\mathbf{q}_i$ are defined by

$$\mathbf{p}_i^{\mathrm{H}}(\mathbf{S}_2 - p_i\mathbf{S}_1) = 0 \qquad \mathbf{p}_i \in \mathrm{range}(\mathbf{S}_1) \tag{55}$$

$$(\mathbf{S}_2 - p_i\mathbf{S}_1)\mathbf{q}_i = 0 \qquad \mathbf{q}_i \in \mathrm{range}(\mathbf{S}_1^H). \tag{56}$$

To find $\mathbf{p}_i$ and $\mathbf{q}_i$, we need to observe the following. Using (16) in (47) yields

$$\mathbf{S}_{efb} = \mathbf{E}_c\mathbf{B}_a\mathbf{E}_r' \tag{57}$$

where

$$\mathbf{B}_a = \mathrm{diag}(|b_1|, |b_2|, \ldots, |b_I|) \tag{58}$$

$$\mathbf{E}_r' = [\mathbf{B}_p\mathbf{Q}_r, \mathbf{E}_d^*\mathbf{Q}_r^*] \tag{59}$$

$$\mathbf{B}_p = \mathrm{diag}[\exp(j\arg(b_1)), \exp(j\arg(b_2)), \ldots, \exp(j\arg(b_I))] \tag{60}$$

$$\mathbf{E}_d = \mathbf{B}_p\mathbf{P}_d^{K-1}\mathbf{Q}_d^{L-1}. \tag{61}$$

Then it follows that

$$\mathbf{S}_1 = \mathbf{E}_{c1}\mathbf{B}_a\mathbf{E}_r \tag{62}$$

$$\mathbf{S}_2 = \mathbf{E}_{c1}\mathbf{P}_d\mathbf{B}_a\mathbf{E}_r \tag{63}$$

where

$$\mathbf{E}_{c1} = \mathbf{E}_c \text{ with the last } L \text{ rows deleted.} \tag{64}$$

Using (62) and (63) in (55) and (56) yields [7] that

$$\begin{bmatrix} \mathbf{p}_1^{\mathrm{H}} \\ \mathbf{p}_2^{\mathrm{H}} \\ \cdots \\ \mathbf{p}_I^{\mathrm{H}} \end{bmatrix} = \mathbf{E}_{c1}^+ = (\mathbf{E}_{c1}^{\mathrm{H}}\mathbf{E}_{c1})^{-1}\mathbf{E}_{c1}^{\mathrm{H}} \tag{65}$$

$$[\mathbf{q}_1, \mathbf{q}_2, \ldots, \mathbf{q}_I] = \mathbf{E}_r^+ = \mathbf{E}_r^{\mathrm{H}}(\mathbf{E}_r\mathbf{E}_r^{\mathrm{H}})^{-1} \tag{66}$$

where + denotes the pseudoinverse.

Using (65), (66), and (62) yields

$$\mathbf{p}_i^{\mathrm{H}}\mathbf{S}_1\mathbf{q}_i = |b_i|. \tag{67}$$

Hence, (54) reduces to

$$\Delta p_i = \frac{1}{|b_i|}\mathbf{p}_i^{\mathrm{H}}(\Delta\mathbf{S}_2 - p_i\Delta\mathbf{S}_1)\mathbf{q}_i. \tag{68}$$

To further simplify (68), it should be noted that

$$\Delta\mathbf{S}_1 = \mathbf{S}_1 \text{ with } s(m,n) \text{ replaced by } w(m,n) \tag{69}$$

and

$$\Delta\mathbf{S}_2 = \mathbf{S}_2 \text{ with } s(m,n) \text{ replaced by } w(m,n). \tag{70}$$

Define two $(K-1)L \times KL$ matrices:

$$\mathbf{P}_t = [\mathbf{I}_{(K-1)L\times(K-1)L}, \mathbf{O}_{(K-1)L\times L}] \tag{71}$$

$$\mathbf{P}_b = [\mathbf{O}_{(K-1)L\times L}, \mathbf{I}_{(K-1)L\times(K-1)L}] \tag{72}$$

where $\mathbf{O}_{(K-1)L\times L}$ is the zero matrix with the given dimension, and $\mathbf{I}_{(K-1)L\times(K-1)L}$ is the identity matrix with the given dimension. Then we can write

$$\Delta\mathbf{S}_1 = \mathbf{P}_t \Delta\mathbf{S}_{efb} \tag{73}$$

$$\Delta\mathbf{S}_2 = \mathbf{P}_b \Delta\mathbf{S}_{efb} \tag{74}$$

where

$$\Delta\mathbf{S}_{efb} = [\Delta\mathbf{S}_e, \mathbf{P}_p \Delta\mathbf{S}_e^*] \tag{75}$$

$$\Delta\mathbf{S}_e = \mathbf{S}_e \text{ with } s(m,n) \text{ replaced by } w(m,n). \tag{76}$$

Using (73) and (74) in (68) leads to

$$\begin{aligned}\Delta p_i &= \frac{1}{|b_i|}\mathbf{p}_i^{\mathrm{H}}(\mathbf{P}_b - p_i\mathbf{P}_t)\Delta\mathbf{S}_{efb}\mathbf{q}_i \\ &= \frac{1}{|b_i|}\mathbf{p}_i^{\mathrm{H}}(\mathbf{P}_b - p_i\mathbf{P}_t)(\Delta\mathbf{S}_e, \mathbf{P}_p\Delta\mathbf{S}_e^*)\mathbf{q}_i.\end{aligned} \tag{77}$$

To express Δp_i in terms of the noise vector $\mathbf{w}$, we first write

$$\mathbf{q}_i = \begin{bmatrix}\mathbf{q}_i' \\ \mathbf{q}_i''\end{bmatrix} \tag{78}$$

where both $\mathbf{q}_i'$ and $\mathbf{q}_i''$ have the dimension $(M-K+1)(N-L+1)\times 1$. Then we can write

$$(\Delta\mathbf{S}_e, \mathbf{P}_p\Delta\mathbf{S}_e^*)\mathbf{q}_i = \mathbf{Q}_i'\mathbf{w} + \mathbf{P}_p\mathbf{Q}_i''\mathbf{w}^* \tag{79}$$

where $\mathbf{Q}_i'$ and $\mathbf{Q}_i''$ are determined by $\mathbf{q}_i'$ and $\mathbf{q}_i''$, respectively, as follows. To define $\mathbf{Q}_i'$, we first write

$$\mathbf{q}_i' = \begin{bmatrix}\mathbf{q}_{i0}' \\ \mathbf{q}_{i1}' \\ \cdots \\ \mathbf{q}_{iM-K}'\end{bmatrix} \tag{80}$$

where

$$\mathbf{q}_{ij}' = \begin{bmatrix} q_{ij0}' \\ q_{ij1}' \\ \cdots \\ q_{ijN-L}'\end{bmatrix}. \tag{81}$$

Then we write

$$\mathbf{Q}_i' = \begin{bmatrix}\mathbf{Q}_{i0}' & \mathbf{Q}_{i1}' & \cdots & \cdots & \mathbf{Q}_{iM-K}' & & & \\ & \mathbf{Q}_{i0}' & \mathbf{Q}_{i1}' & \cdots & \cdots & \mathbf{Q}_{iM-K}' & & \\ & & \cdots & \cdots & \cdots & \cdots & \cdots & \\ & & & \mathbf{Q}_{i0}' & \mathbf{Q}_{i1}' & \cdots & \cdots & \mathbf{Q}_{iM-K}'\end{bmatrix} \tag{82}$$

where

$$\mathbf{Q}_{ij}' = \begin{bmatrix} q_{ij0}' & q_{ij1}' & \cdots & \cdots & q_{ijN-L}' & & & \\ & q_{ij0}' & q_{ij1}' & \cdots & \cdots & q_{ijN-L}' & & \\ & & \cdots & \cdots & \cdots & \cdots & \cdots & \\ & & & q_{ij0}' & q_{ij1}' & \cdots & \cdots & q_{ijN-L}'\end{bmatrix} \tag{83}$$

Note that in (82) and (83), zeros should be inserted into the lower-left and upper-right triangles. $\mathbf{Q}_i''$ is similarly defined as $\mathbf{Q}_i'$.

Using (79) in (77) and then (77) in (51) yields that

$$\begin{aligned}\Delta f_{xi} = {}& \frac{1}{2\pi|b_i|}\mathrm{Im}\left[\frac{1}{p_i}\mathbf{p}_i^{\mathrm{H}}(\mathbf{P}_b - p_i\mathbf{P}_t)(\mathbf{Q}_i' + P_pQ_i'')\right]\mathrm{Re}[\mathbf{w}] \\ &+ \frac{1}{2\pi|b_i|}\mathrm{Re}\left[\frac{1}{p_i}\mathbf{p}_i^{\mathrm{H}}(\mathbf{P}_b - p_i\mathbf{P}_t)(\mathbf{Q}_i' - P_pQ_i'')\right]\mathrm{Im}[\mathbf{w}].\end{aligned} \tag{84}$$

Hence, it follows that

$$\epsilon_{xi1}^T = \frac{1}{2\pi|b_i|}\mathrm{Im}\left[\frac{1}{p_i}\mathbf{p}_i^{\mathrm{H}}(\mathbf{P}_b - p_i\mathbf{P}_t)(\mathbf{Q}_i' + P_pQ_i'')\right] \tag{85}$$

$$\epsilon_{xi2}^T = \frac{1}{2\pi|b_i|}\mathrm{Re}\left[\frac{1}{p_i}\mathbf{p}_i^{\mathrm{H}}(\mathbf{P}_b - p_i\mathbf{P}_t)(\mathbf{Q}_i' - P_pQ_i'')\right]. \tag{86}$$

To obtain ϵ_{yi1} and ϵ_{yi2}, all we need to do is to interchange p_i and q_i, M and N, and K and L inherent in (85) and (86).

Assume that the noise vector $\mathbf{w}$ is white, i.e.,

$$E\{\mathrm{Re}[\mathbf{w}]\mathrm{Re}[\mathbf{w}]^T\} = \sigma^2\mathbf{I} \tag{87}$$

$$E\{\mathrm{Im}[\mathbf{w}]\mathrm{Im}[\mathbf{w}]^T\} = \sigma^2\mathbf{I} \tag{88}$$

$$E\{\mathrm{Re}[\mathbf{w}]\mathrm{Im}[\mathbf{w}]^T\} = 0 \tag{89}$$

where $E\{\ \}$ denotes the expectation. Then the variances of the perturbations Δf_{xi} and Δf_{yi} are

$$\mathrm{var}(\Delta f_{xi}) = \sigma^2[\|\epsilon_{xi1}\|^2 + \|\epsilon_{xi2}\|^2] \tag{90}$$

$$\mathrm{var}(\Delta f_{yi}) = \sigma^2[\|\epsilon_{yi1}\|^2 + \|\epsilon_{yi2}\|^2] \tag{91}$$

where $\|\ \|$ denotes the 2-norm. It is easy to show (by observing (85), (86), (90), and (91)) that the normalized perturbation variances, i.e., $\mathrm{var}(\Delta f_{xi})\mathrm{SNR}_i$ and $\mathrm{var}(\Delta f_{yi})\mathrm{SNR}_i$ where $\mathrm{SNR}_i = |b_i|^2/2\sigma^2$ (SNR is signal-to-noise ratio) are independent of the noise level σ^2 and all the signal amplitudes $|b_j|$ for $j = 1,\ldots,I$.

More insights into the perturbation variances remain to be found through analysis. In the following subsection, we show some numerical results.

B. Numerical Results

Figs. 3(a)–(b) show the 3-D and 2-D plots of the perturbation variance (in dB) of f_{x1} versus the window lengths K and L for the single scatterer case where $I = 1$, $M = N = 20$, and $\arg(b_1)$, f_{x1} and f_{y1} are

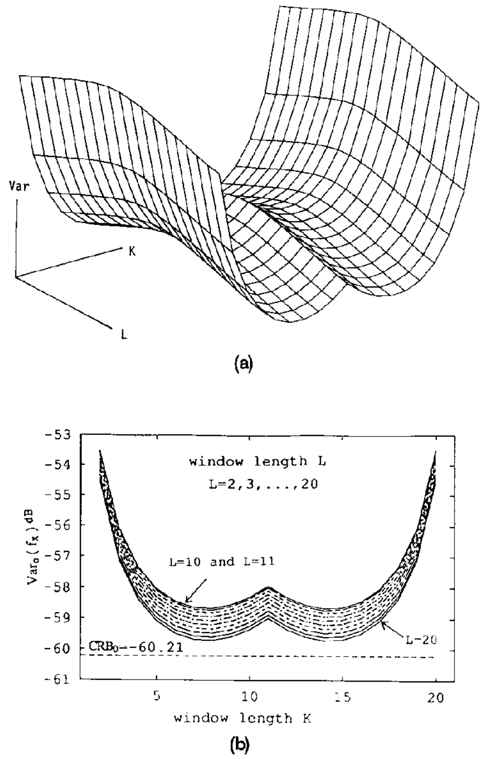

Fig. 3. Normalized perturbation variance of f_{x1} versus K and L for single scatterer case. (a) 3-D plot. (b) 2-D plot.

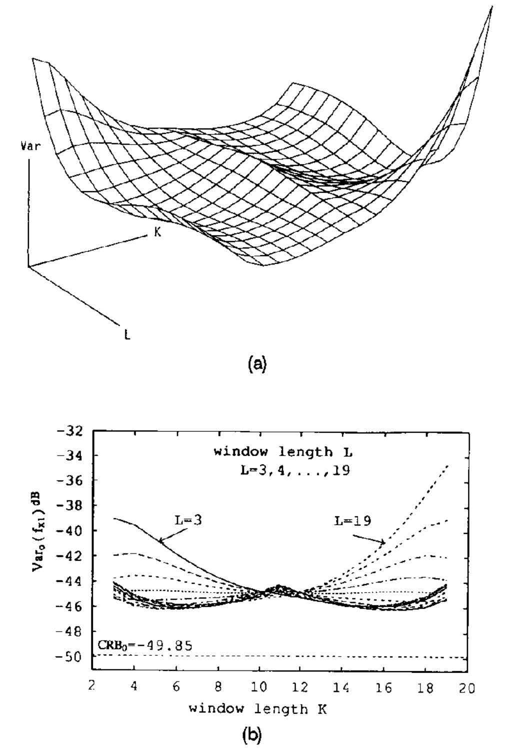

Fig. 4. Normalized perturbation variance of f_{x1} or f_{x2} versus K and L for two scatterers case. (a) 3-D plot. (b) 2-D plot.

arbitrary. From these two plots, we can see that the optimum choices of K and L are, respectively, $K = m/3$ or $K = 2M/3$, and $L = I + 1$ or $L = N - I + 1$; the perturbation variance of f_x is affected more by K than L (and similarly the perturbation variance of f_y is affected more by L than K); and with proper choices of K and L, the perturbation variance is very close to the CRB.

Note that the CRB [9] was computed by assuming that the additive noise is white Gaussian and the unknown parameters are $|b_i|$, $\arg(b_i)$, f_{xi} and f_{yi} for $i = 1, \ldots, I$.

Figs. 4(a)–(b) show the 3-D and 2-D plots of the perturbation variance (in dB) of f_{x1} or f_{x2} versus K and L for the two scatterers case where $I = 2$, $M = N = 20$, $\arg(b_i) = \arg(b_2) = 0$, $(f_{x1}, f_{y1}) = (0.24, 0.26)$ and $(f_{x2}, f_{y2}) = (0.26, 0.24)$. Note that $\mathrm{var}(f_{x1})\mathrm{SNR}_1$ has been found to be identical to $\mathrm{var}(f_{x2})\mathrm{SNR}_2$ for this case. These two plots suggest that the boundary values of K and L (i.e., the values close to $I + 1$ for both K and L as well as those close to $M - I + 1$ and $N - I + 1$ for K and L respectively), should be avoided.

Figs. 5(a)–(f) show the 3-D and 2-D plots of the perturbation variances (in dB) of f_{x1}, f_{x2}, and f_{x3} for the three scatterers case where $I = 3$, $M = N = 20$, $\arg(b_1) = \arg(b_2) = \arg(b_3) = 0$, $(f_{x1}, f_{y1}) = (0.24, 0.26)$, $(f_{x2}, f_{y2}) = (0.26, 0.24)$ and $(f_{x3}, f_{y3}) = (0.24, 0.24)$. These figures again suggest that the boundary values of K and L should be avoided.

From the above numerical results (as well as others not shown here), we conclude that the optimum choices of K and L are generally data dependent, but the choices away from the boundary values of K and L are generally good. As a rule of thumb, one can simply choose $K = M/2$ and $L = N/2$ for a good noise sensitivity performance.

V. SIMULATION RESULTS

It has been shown that for data satisfying the model shown in (2), the MP method can yield the exact estimates of the scatterer positions and it also has a good noise sensitivity performance. In this section, we test the MP method for data that does not satisfy (2) but rather the more realistic model (1). To do the test, we assume the following.

The target is continuously rotating at the speed of 20 deg/s. For every 17.97 μs, the radar transmits a pulse at a stepped frequency. The stepped frequency (in x-band) varies from 9 GHz to 9.24 GHz in 32 steps (i.e., the step length is 7.81 MHz). The sequence of such 32 pulses are repeatedly transmitted by the radar towards the target for 32 times (sweeps). The distance

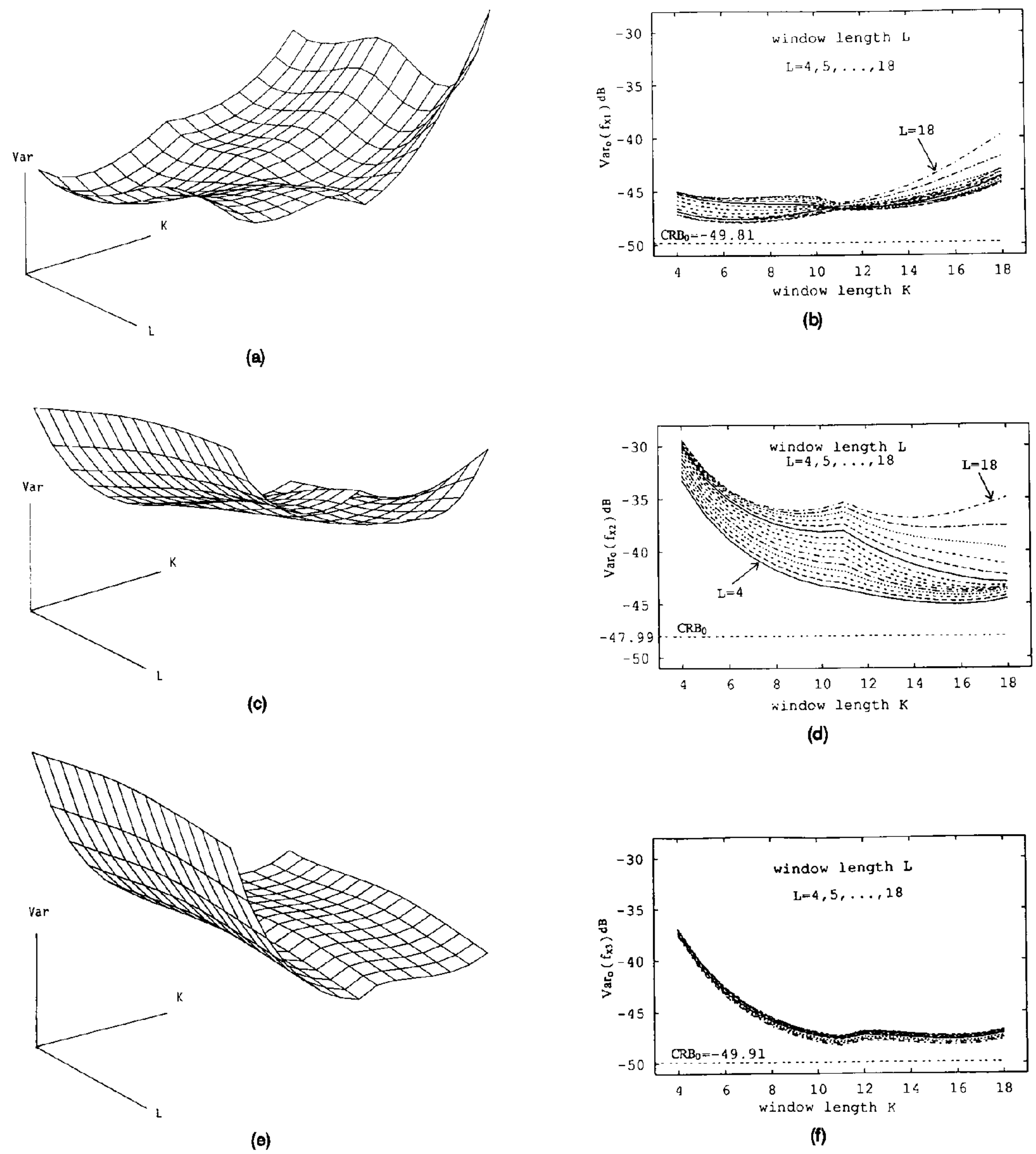

Fig. 5. Normalized perturbation variances versus K and L for three scatterers case. (a) 3-D plot for f_{x1}. (b) 2-D plot for f_{x1}. (c) 3-D plot for f_{x2}. (d) 2-D plot for $fx2$. (e) 3-D plot for f_{x3}. (f) 2-D plot for f_{x3}.

between the target and the radar is assumed to be a known constant during the observation time so that the phase due to the distance can be compensated (i.e., set $d = 0$ in (1)). The scatterers in the target are assumed to have identical reflection coefficients (i.e., $a_i = 1$) and form an angular shape as shown in Fig. 8. (Note that (x_i, y_i) can be easily converted from (f_{xi}, f_{yi}) by using (4) and (5).) Using the above assumptions in (1), we obtained a 32×32 synthesized ISAR data set. Furthermore, a white noise was added to the data and the SNR was -10 dB (i.e., $\mathrm{SNR}_i = 10\log_{10}|a_i|^2/2\sigma^2 = -10$ where $|a_i|$ is the amplitude of the reflection coefficient and $2\sigma^2$ the noise variance.).

Figs. 6(a)–(b) show the 3-D and contour plots of the Fourier spectrum of the synthesized data set. The scatterers are not very noticeable from the two plots. This is because of the small aperture of the available data set. Note that the split ellipses around each peak position shown in the contour plot are due to the sidelobes around each mainlobe as shown in the 3-D plot.

Figs. 7(a)–(b) show the 3-D and contour plots of the high resolution spectrum defined by (28). These two plots clearly show the scatterers.

Fig. 8 shows the estimated scatterer positions (marked by "o") obtained by the MP method. Note

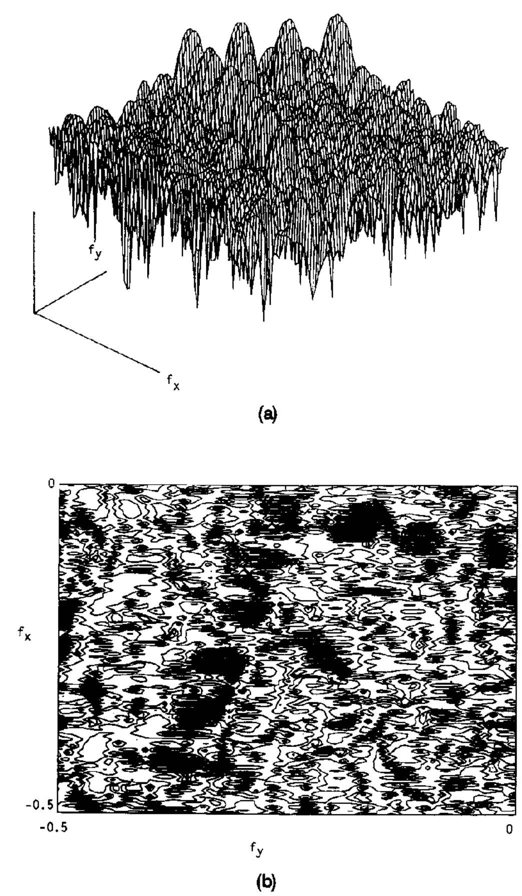

Fig. 6. Fourier transform of synthesized ISAR data. (a) 3-D plot of 2-D DFT using synthetic ISAR data (SNR = -10 dB). (b) Contour map of 2-D DFT using synthetic ISAR data (SNR = -10 dB).

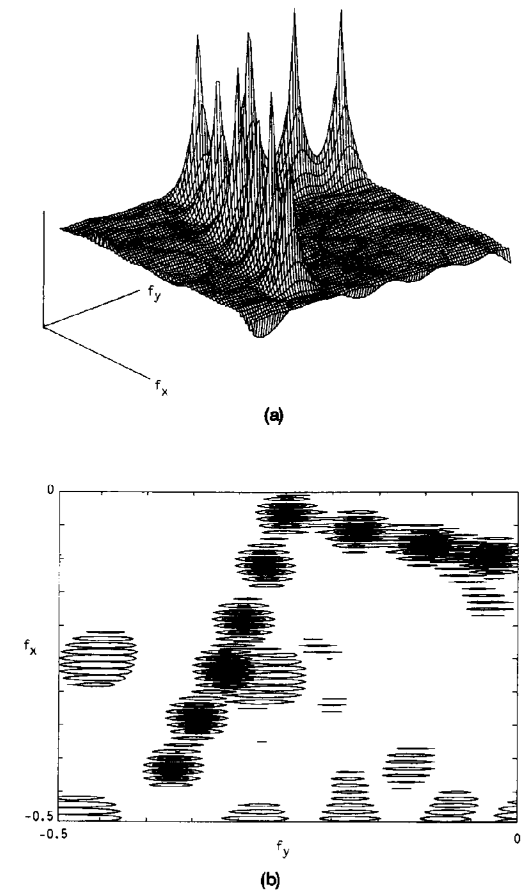

Fig. 7. High resolution spectrum of synthesized ISAR data. (a) 3-D plot. Frequency spectrum using synthetic ISAR data (SNR = -10 dB). (b) Contour map of frequency spectrum using synthetic ISAR data.

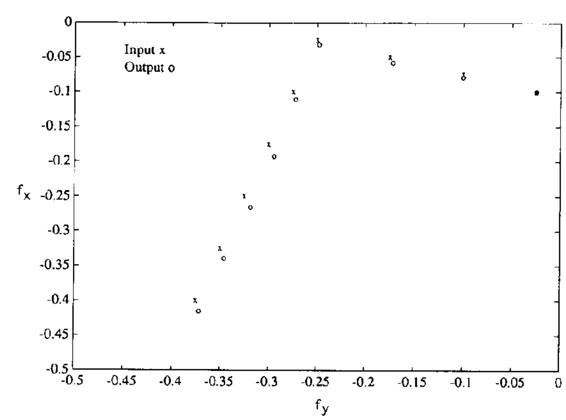

Fig. 8. Original and estimated scatterer positions. MP on synthetic ISAR data (SNR = -10 dB).

that the estimated scatterer positions are basically the peak positions of the high resolution spectrum shown in Fig. 7, but they were obtained by using the MP method which is computationally much more efficient than searching for peak positions in the high resolution spectrum. The original scatterer positions are marked by "x". From this figure, we can see a deviation of the estimated positions from the original. This deviation appears to be a rotation of the target around its origin (i.e., the upper right-hand corner of this figure). In fact, we observed in our simulation that this rotation was caused by the model errors between (1) and (2), and the added noise caused little perturbations in the estimated positions. However, when the SNR was reduced to -15 dB, the pairing step in the MP method failed and it produced a drastically different picture.

VI. CONCLUSIONS

We have presented a computationally efficient and high resolution method, i.e., the MP method, for localization of point scatterers in a moving target from ISAR data. We have provided a noise sensitivity analysis of this method and shown that its performance is near optimum. We have also tested this method using a relatively realistic synthesized ISAR data set and shown that this method is fairly robust to model errors. Based on the theory shown in this paper, the application of this method to real life ISAR data (like data from moving ships and flying aircrafts) is currently under investigation.

REFERENCES

[1] Chen, C-C., and Andrew, H. C. (1980)
Multifrequency imaging of radar turntable data.
IEEE Transactions on Aerospace and Electronic Systems, **AES-16**, 1 (Jan 1980), 15–22.

[2] Steinberg, B. D. (1988)
Microwave imaging of aircraft.
IEEE Proceedings, **76**, 12 (Dec. 1988), 1578–1592.

[3] Hua, Y. (1991)
Estimating two-dimensional frequencies by matrix enhancemanent and matrix pencil.
In *Proceedings of the International Conference on Acoustics, Speech, and Signal Processing* (ICASSP91), Toronto, Canada, May 1991.

[4] Marple, S. L. (1987)
Digital Spectral Analysis with Applications.
Englewood Cliffs, NJ: Prentice-Hall, 1987.

[5] Nash, G., and Nandagopal, D. (1990)
Signal processing techniques for radar imaging.
In *Proceedings of the First Australian Radar Conference (Radarcon90)*, Adelaide, Australia, Apr. 1990.

[6] Hua, Y., and Sarkar, T. K. (1991)
On SVD for estimating generalized eigenvalues of singular matrix pencil in noise.
IEEE Transactions on Signal Processing, **37**, 4 (Apr. 1991), 892–900.

[7] Hua, Y., and Sarkar, T. K. (1990)
Matrix pencil method for estimating parameters of exponentially damped/undamped sinusoids in noise.
IEEE Transactions on Acoustics, Speech, and Signal Processing, **36**, 5 (May 1990), 814–824.

[8] Golub, G. H., and Van Loan, C. F. (1983)
Matrix Computations.
Baltimore, MD: Johns Hopkins University Press, 1983.

[9] Van Trees, H. L. (1968)
Detection, Estimation and Modulation Theory, Part I.
New York: Wiley, 1968.

Yingbo Hua (S'86—M'87—SM'92) was born in Wu-Xi, Jiangsu, China, on Nov. 26, 1960. He received the B.S. degree in control engineering from Southeast University (Nanjing Institute of Technology), Nanjing, Jiangsu, China, in 1982, and the M.S. and Ph.D. degrees in electrical engineering from Syracuse University, Syracuse, NY, in 1983 and 1988, respectively.

He was a Graduate Teaching Assistant from 1984 to 1985, a University Graduate Fellow from 1985 to 1986, a Graduate Research Assistant from 1986 to 1988, and a Postdoctoral Research Associate from 1988 to 1989, all at Syracuse University. Since early 1990, he has been a Lecturer with the University of Melbourne, Victoria, Australia. He has contributed over 40 publications. His current interests include spectral estimation, array processing, and radar imaging.

Farhan A. Baqai was born in Karachi, Pakistan on July 26, 1965. He received the B.S. (Honors) degree in electrical engineering from University of Engineering and Technology, Lahore, Pakistan, in 1989. Currently he is a Masters student in the Department of Electrical and Electronic Engineering, The University of Melbourne, Australia.

From 1989 to 1991 he worked as a Research Engineer in the Research and Development department of Carrier Telephone Industries (Pvt) Ltd., Islamabad, Pakistan. His principal duties involved the design and development of telecommunication equipment. His graduate work at the University of Melbourne is in the general area of digital signal processing and radar imaging.

Yan Zhu was born in Nanjing, China, on July 13, 1963. She received the B.S. degree in control engineering from Nanjing Institute of Technology (now called Southeast University), China, in 1985.

She was a Lecturer Assistant at Nanjing Power Institute, China, from 1985 to 1990. Since January 1991, she has been a Research Assistant at the University of Melbourne, Victoria, Australia.

David J. Heilbronn received a B.Sc. (hons) in 1971 and a Ph.D. degree in 1975 from the University of Melbourne, Australia.

He has worked at DSTO Salisbury, Australia since 1975 in areas of image sensors and processing, HF radar and microwave radar. He spent 1983–1985 with Radar Systems Group, Hughes Aircraft Co., Los Angeles and then returned to DSTO. Since then he has worked in radar systems, target identification, SAR and ISAR and he has published a number of papers in these fields. He is currently the Research Leader of the Microwave Radar Division, DSTO.